Cryogenic preamplification of a single-electron-transistor using a silicon-germanium heterojunction-bipolar-transistor

M. J. Curry, T. D. England, N. C. Bishop, G. Ten-Eyck, J. R. Wendt, T. Pluym, M. P. Lilly, S. M. Carr, and M. S. Carroll

Citation: Appl. Phys. Lett. **106**, 203505 (2015); doi: 10.1063/1.4921308
View online: https://doi.org/10.1063/1.4921308
View Table of Contents: http://aip.scitation.org/toc/apl/106/20
Published by the American Institute of Physics

Cryogenic preamplification of a single-electron-transistor using a silicon-germanium heterojunction-bipolar-transistor

M. J. Curry,[1,2,3] T. D. England,[3] N. C. Bishop,[3] G. Ten-Eyck,[3] J. R. Wendt,[3] T. Pluym,[3] M. P. Lilly,[3] S. M. Carr,[2,3] and M. S. Carroll[3]
[1]*Department of Physics and Astronomy, University of New Mexico, Albuquerque, New Mexico 87131, USA*
[2]*Center for Quantum Information and Control, University of New Mexico, Albuquerque, New Mexico 87131, USA*
[3]*Sandia National Laboratories, 1515 Eubank Blvd SE, Albuquerque, New Mexico 87123, USA*

(Received 13 March 2015; accepted 6 May 2015; published online 21 May 2015)

We examine a silicon-germanium heterojunction bipolar transistor (HBT) for cryogenic pre-amplification of a single electron transistor (SET). The SET current modulates the base current of the HBT directly. The HBT-SET circuit is immersed in liquid helium, and its frequency response from low frequency to several MHz is measured. The current gain and the noise spectrum with the HBT result in a signal-to-noise-ratio (SNR) that is a factor of 10–100 larger than without the HBT at lower frequencies. The transition frequency defined by SNR = 1 has been extended by as much as a factor of 10 compared to without the HBT amplification. The power dissipated by the HBT cryogenic pre-amplifier is approximately 5 nW to 5 μW for the investigated range of operation. The circuit is also operated in a single electron charge read-out configuration in the time-domain as a proof-of-principle demonstration of the amplification approach for single spin read-out. © *2015 AIP Publishing LLC*. [http://dx.doi.org/10.1063/1.4921308]

Donor spin qubits have recently received increased interest because of the demonstration of high fidelity coherent control of phosphorus donors using a local electron spin resonance technique.[1,2] This approach is of interest both for quantum information[3–5] as well as representing a new experimental platform to investigate the behavior of single impurities in semiconductors using electron and nuclear magnetic resonance. Single-shot readout[6–8] of the spin polarization is an important component of the measurement. It may be accomplished using a wide-band measurement of the single electron transistor[9] (SET) conductance, which is sensitive to the ionization condition of any nearby donors.[10,11] The technique relies on alignment of the neighboring SET chemical potential between discrete Zeeman energy levels. The donor spin-up electron ionizes into the SET, leading to a detectable transient change in the local electrostatic potential, while a SET electron waits to reload into the donor as a spin-down. The temporary ionization of the donor changes the conductance of the SET, which is measured as a current pulse corresponding to a spin-up electron or no pulse if the electron was spin-down.

Read-out fidelity can be no better than what the signal-to-noise-ratio (SNR) provides for a particular bandwidth, although other factors can introduce errors that degrade the fidelity such as rapid tunneling events that are faster than the bandwidth of the read-out. The donor read-out technique is performed at cryogenic temperatures less than 4 K, which is typically necessary to observe the spin read-out of the donor state at reasonably low magnetic fields. The SET current is subsequently amplified at room-temperature (RT) using one or several amplification stages, typically including a transconductance amplifier. The line capacitance between the transconductance amplifier and the SET typically sets the limits of performance of the circuit. Increased read-out bandwidth can improve fidelity, for example, by detecting faster tunnel events, however, the increased bandwidth reduces SNR. The SNR can be increased if amplification is introduced before the dominant noise source contributes to the signal.

Several approaches have been pursued to maximize SNR using cryogenic electronics for read-out and amplification. One technique is to embed an SET in a RF resonant circuit, referred to as RF-SET,[12–14] which has resulted in some of the most competitive read-out performance. However, the RF-SET technique requires a significant investment to implement, it introduces some challenges to integration,[15–17] and for the purpose of donor spin read-out it can introduce an additional complication of directly modulating the chemical potential of the SET. An alternative technique, similar in some respects to the RF-SET approach, is to couple a SET or similar device to a superconducting resonator,[18–20] which may be followed by additional superconducting quantum circuitry such as a Josephson Parametric Amplifier.[21–23] Current comparators have shown promise but their thresholds of sensitivity have been near the limits of the current output of SETs, making them difficult to implement without a preamplification stage.[24,25] Cryogenic preamplification using discrete high-electron-mobility-transistors (HEMTs) has been investigated resulting in sufficient SNR for a particular bandwidth.[26] However, HEMTs may require a relatively high power dissipation, and the typical circuit configuration introduces a fixed load resistance in front of the gate that can limit the circuit bandwidth.

In this letter, we use a discrete, commercial silicon-germanium (SiGe) heterojunction bipolar transistor[27–31] (HBT) for cryogenic[32,33] amplification of a silicon SET's output current. This is a preamplification stage for a single electron spin read-out circuit. The SiGe HBT can be operated at relatively low power, has a low overhead for implementation,

and, in principle, could be integrated with a silicon-based qubit process flow. We find that the HBT provides a current gain of order 100–2000. The current gain and the noise spectrum with the HBT result in a SNR that is a factor of 10–100 larger than without the HBT at lower frequencies. The transition frequency defined by SNR = 1 has been extended by as much as a factor of 10 compared to without the HBT amplification. The power dissipated by the HBT is estimated to be between 5 nW and 5 μW for the relevant operation range.

The measurement circuit with both HBT and SET is shown in Figure 1. The base of the HBT is connected to the source of the SET using a bond wire between a surface mount HBT and the SET chip, both of which are immersed in liquid helium during measurement. The HBT collector is connected to a one meter long Lakeshore 304 stainless steel braided coaxial cable with a capacitance of approximately 174 pF/m. The emitter is connected via an identical cable to either a Keithley 2400 or an Agilent 33500B for low and high frequency measurements, respectively. The gate labeled V_A is also connected to coaxial cables for pulsed measurements, while all other leads were connected through twisted pair lines. The HBT collector is connected to a room-temperature Femto DLPCA-200 transimpedance preamplifier unless otherwise noted. A subsequent SR560 voltage preamplifier is used as a variable bandwidth filter but otherwise is set to a gain of 1. Lock-in measurements were done with a Zurich HF2LI or SR830 using a 100:1 resistive voltage divider and typically an excitation voltage of 100 μV or 1 mV on the SET drain, without or with the HBT, respectively, unless otherwise noted. The DC bias was set by the DC source applied to the HBT emitter with no voltage division.

HBTs were first characterized in liquid helium with room-temperature load resistors without the SET to simulate different SET resistances and calibrate the transistor's collector current as a function of base current and load resistance, Figure 2. Multiple commercially available high bandwidth HBTs were measured at low temperature. Resistances between 100 kΩ and 1 GΩ were examined. The DC behavior of these HBTs at low

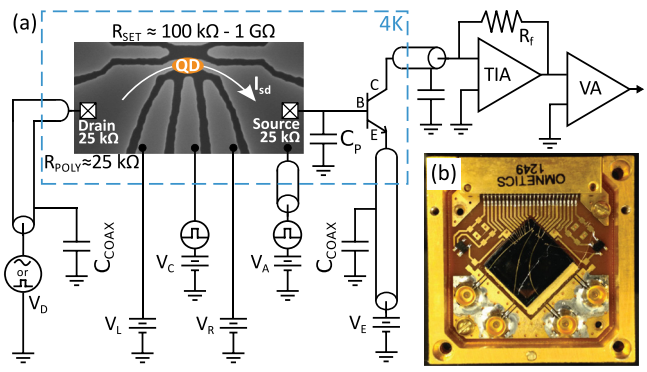

FIG. 1. The HBT-SET circuit. The SEM image shows the silicon metal-oxide-semiconductor device geometry with polysilicon gates labeled V_L, V_C, V_R, and V_A. The QD is formed beneath the narrow channel of the gate labeled V_A. The circuit is DC biased by V_E and AC biased by V_D (either sinusoidal or pulsing inputs). The parasitic capacitance, C_P, is due to the device and/or PCB. The parasitic capacitance, C_{COAX}, is due to the length of the wires leading to and from the device immersed in liquid helium at 4 K. Room-temperature transimpedance (TIA) and voltage (VA) amplifiers are used to amplify the signal before it is read out on a lock-in amplifier or oscilloscope.

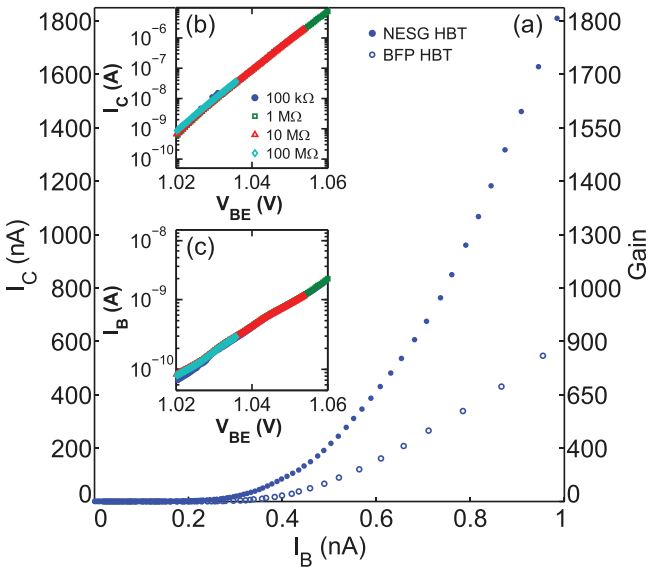

FIG. 2. HBT biasing calibration curves at 4 K. (a) Collector current as a function of base current for the CEL NESG3031M05 HBT used and an Infineon BFP842ESD HBT. This curve enables mapping from read-out current to device input current regardless of SET resistance. The gain shown is for the NESG HBT. (b) Collector current as a function of the HBT base-emitter voltage for different resistors in-line with an NESG HBT. Identical HBT turn-on behavior is observed regardless of the load resistance before the base-emitter junction of the HBT. (c) Base current as a function of the HBT base-emitter voltage for different resistors in-line with an NESG HBT. These current curves similarly overlap.

temperature is exponential. As the input current, I_B, increases, the readout current, I_C, increases exponentially, Figure 2(a). The turn-on behavior of the HBT in our circuit depends solely on the forward-bias diode drop across the base-emitter (BE) junction, V_{BE}. V_{BE} is calculated by subtracting the voltage drop across the resistor from the bias applied to the emitter. For different resistances, input and readout current behave exactly the same as V_{BE} is increased, Figures 2(b) and 2(c). Therefore, for a given readout current, the input current is known and by using this curve as a calibration, the potential across a SET connected to the HBT, for a fixed emitter bias, can be estimated as $\triangle V_{SET}(I_C) = |V_E| - |V_{BE}(I_C)|$. We note that not all HBTs measured at 4 K showed greater than unity current gain ($I_C/I_B > 1$) combined with correspondingly low voltage of 0.1–2 mV across the test resistance. Typical operation of the silicon SETs for read-out is done with a bias voltage of 80–300 μV, well below the charging energy of the SET to avoid reduction of sensitivity from broadening of the Coulomb blockade peaks. Out of 25 HBTs characterized at 4 K, the California Eastern Laboratories (CEL) NESG3031M05 (Ref. 34) HBT showed the highest current gain and lowest test resistance biasing, so it was selected for measurements with the SET.

To examine the frequency response of the SET with and without the HBT, narrow band lock-in measurements were done by inputting a small voltage sinusoidal signal into the SET's drain resulting in a sinusoidal input current, i_b, and a sinusoidal readout current, i_c. To ensure the DC operating point was minimally perturbed, input signal magnitudes were constrained to $i_c \leq 0.2 \cdot I_C$, remaining within a linear signal regime. A set of charge stability plots show Coulomb blockade through the quantum dot (QD), Figures 3(a)–3(c).

The stability plots are formed by sweeping the center plunger, V_C, and stepping the left and right plungers, $V_{L,R}$, as indicated in Figure 1. Qualitatively, the presence of Coulomb blockade confirms that a DC bias can be chosen that produces V_{SD} sufficiently below the charging energy of the QD. We estimate that V_{SD} for $V_E = -1.051$ V is approximately 1 mV, extracted from the appropriate I_C vs V_{BE} curve.

The SET-HBT current does not go to zero in the blockaded regions. Verilog-A simulations of the circuit including a model for SET conductance and the calibrated 4 K HBT parameters[35] predict that the HBT-SET minimum conductance for the Coulomb blockade will be prevented from going to zero. This behavior is believed to be a consequence of having a floating source that increases V_{SD} to maintain some current through both the HBT and SET at all times. That is, relatively small changes in the DC bias current through the HBT lead to relatively large voltage shifts from V_{BE} to V_{SD}. The current turn-off of the Coulomb blockade is consequently suppressed because the shift of voltage drop from V_{BE} to V_{SD} is always enough to maintain a small current through both the SET and the HBT. Quantum point contacts (QPCs) are also frequently used as charge sensors and would likely minimize this complication of the amplification circuit. That is, the conductance of a QPC varies much less over similar bias ranges, and usually very low conductance conditions can be avoided.

Quantitatively, the cases with and without the HBT are compared for equal input signal, 100 μV, and similar SET resistance, 100 kΩ to 1 MΩ, Figures 3(d)–3(f). The lock-in signal shown is the in-phase quadrature. The frequency dependence of the narrow band SNR is shown for several room-temperature transimpedance amplifier gain settings, Figure 3(f). The current gain and the noise spectrum with the HBT result in a SNR that is a factor of 10–100 larger than without the HBT at lower frequencies. For stability plots such as Figure 3(a), we were able to reduce the lock-in time constant by at least a factor of 10 due to the increased SNR, thereby reducing the total acquisition time by at least the same factor.

In Figure 3(f), the transition frequency, defined by SNR = 1, for the case without the HBT is observed to be ~100 kHz, where |SNR|≪1 for frequencies higher than 100 kHz. The transition frequency is extended with the addition of the HBT. The extended transition frequency with the HBT enabled acquisition of narrow band stability plots at 2 MHz, as shown in Figure 3(c). For frequencies near and beyond approximately 200 kHz in Figure 3(f), a significant shift in phase that approaches 180° is observed in the lock-in detected signal. The absolute value of the signal and SNR is plotted in Figures 3(d) and 3(f) in order to show this phase shift. Circuit analysis of Figure 1(a) indicates that the HBT circuit has a pole due to the SET resistance and the parasitic capacitance, C_P, as well as an additional pole due to the HBT base-collector resistance and the parasitic capacitance of the coaxial cables, C_{COAX}.

The response of the SET-HBT circuit was measured in the time domain by tuning the SET in resonance with a nearby charge center such that tunneling events on/off of the charge center are observed as changes in the conductance of the SET between two conductance states: charge center neutral or ionized, Figures 4(a)–4(c). This is similar to a charge sensing or spin read-out configuration. The magnitude of conductance change is not the largest possible but was chosen in this case because of a combination of factors including the average tunneling rate of the transition. These data were

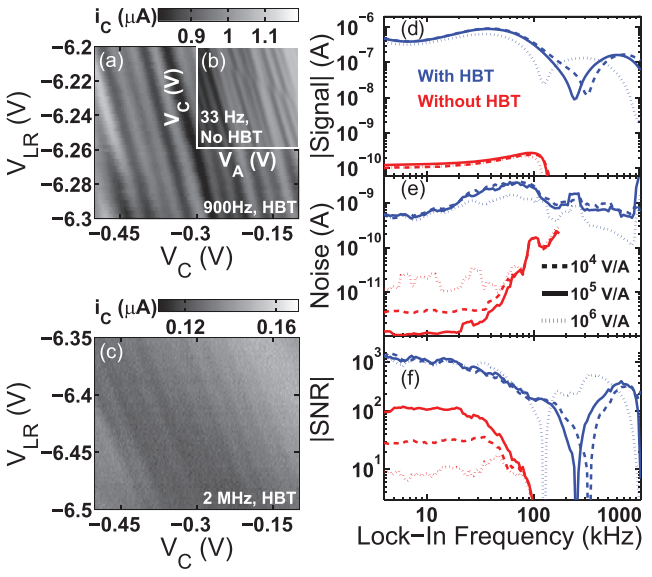

FIG. 3. Stability plots and narrow band frequency domain data. All measurements were performed at a temperature of 4 K. (a) Stability plot showing the SET Coulomb blockade behavior of the HBT-SET circuit at 900 Hz. Well defined peaks and contrast are found when an HBT is added. (b) Stability plot of the same SET and resulting Coulomb blockade with no HBT. Similar contrast to (a) is observed. (c) Stability plot showing the SET Coulomb blockade in a very similar voltage range as (a) but with an input frequency of 2 MHz. The SNR decreases at higher frequencies in this narrow band measurement. (d)–(f) Narrow band measurements as a function of input frequency. All data are the lock-in output's in-phase quadrature. The signal and SNR are plotted as absolute values.

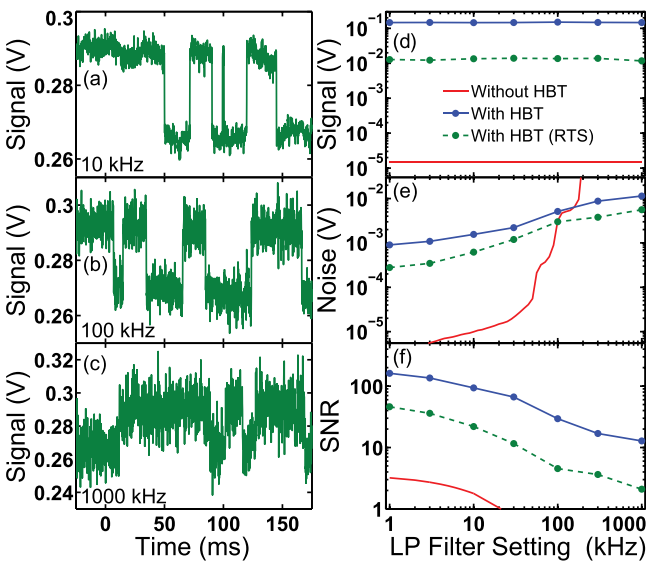

FIG. 4. (a)–(c) Single-shot oscilloscope traces of RTS due to proximal charge center tunneling. Room-temperature low pass filter settings of 10 kHz, 100 kHz, and 1000 kHz are used to monitor the RTS. (d)–(f) Measured wide band signal magnitude, noise magnitude, and SNR as a function of low-pass (LP) filter setting. The blue curves show calibrated input current (150 pA) pulse data for the HBT-SET circuit. The red curve is the same current input as the blue curve with noise calculated from the narrow band noise spectral density for the SET circuit without the HBT. The green curve shows the measured RTS data from Figures 4(a)–4(c).

acquired using a room-temperature amplification chain consisting of a Femto DLPCA-200 transimpedance amplifier with sensitivity 10^5 V/A followed by an SR 560 voltage amplifier with gain of 1 and variable low-pass filter 3-dB frequencies. Measurements of signal amplitude, noise (RMS deviation from the mean value of a voltage level), and SNR are summarized for voltage-amplifier low-pass filter settings up to 1 MHz. Other circuit parasitics introduce signal loss at frequencies less than 1 MHz as indicated by the narrowband measurements, however, SNR > 1 is still achieved at ~1 MHz with the HBT-SET circuit, as shown by the green random telegraph signal (RTS) curve in Figure 4(f).

The circuit response to direct pulsing on the drain ohmic was investigated to more directly examine rise/fall time response. The pulses were generated by applying externally controllable square voltage pulses to the drain ohmic, with the voltage amplitude converted to a current amplitude by measuring and taking the difference of the current at both voltage levels with a current meter. Square pulses with amplitude 150 pA and width 2 ms were used for the uppermost (blue) curve in Figure 4(d). These data were acquired using a RT amplification chain consisting of a Femto DLPCA-200 transimpedance amplifier with sensitivity 10^5 V/A followed by an SR 560 voltage amplifier with a gain of 1 and variable low-pass filter 3-dB frequencies. We found that the conductance of the SET modified the bandwidth of the circuit response and that for the maximum and minimum conductances examined, 0.313 μS and 0.183 μS, respectively, we found response times of 14.5 μs and 0.612 μs, respectively. The SNR from the RTS like behavior is overlaid as green curves. The blue curve in Figure 4(f) shows an improved SNR primarily because the current through the SET is being driven by an external pulse instead of being limited by the change in conductance in the SET from the RTS charge center at a fixed V_{SD} range. Through the calibration of voltage to current, we find a current amplitude of 13 pA for the RTS data in Figs. 4(a)–4(c).

For comparison between the device with and without the HBT, we estimate the wide band SNR from the narrow band measurements. That is, we assume the same current pulse amplitude of 150 pA is used from the uppermost (blue) curve in Figure 4(d), and we calculate the total noise by integrating the noise spectral density that was measured in the narrow band measurements without the HBT. Noise spectral density was calculated by dividing the solid red curve in Figure 3(e) by the square root of the noise-equivalent-power bandwidth of 1.25 Hz, calculated from the lock-in time constant and filter roll-off. The noise spectral density was integrated to an upper limit equal to the voltage amplifier low-pass filter 3-dB frequency, resulting in the red curve in Figure 4(e). We find that the noise increases nonlinearly with the HBT and also for the calculated case without the HBT, while the signal stays constant throughout the low-pass filter setting range. With the HBT, there is an increase in SNR of about a factor of 10 for the RTS case (green) and about a factor of 60 for the direct pulsing case (blue) at lower frequencies. The greater SNR, particularly at lower frequencies, appears to be due to an amplification in signal before the dominant noise source is introduced, perhaps near the input of the preamplifier at room-temperature. The SNR for the direct pulsing (blue) and the RTS (green) is reduced at higher filter settings because of the nonlinearly increasing noise. However, with the HBT, the gain is sufficiently high such that pulsing events are detectable at the microsecond time scale.

An estimate of the DC power dissipation of the HBT can be made by taking the product of the current through and voltage across the HBT. The peak conductance conditions observed in this work correspond to $I_B \approx 1$ nA and $I_C \approx 5$ μA maximum and $|V_E| \approx 1$ V, from which we can estimate a power dissipation of $V{\cdot}I = 1(V) \times 5{\cdot}10^{-6}(A) = 5$ μW. Regions off of peak conductance, that is, most of the stability diagram, correspond to power dissipations as low as 10–100 nW. Even at the highest estimated power of 5 μW, the power dissipation is less than or about equal to the cooling power of the lowest temperature stage of a dilution refrigerator.

We examined a discrete, commercial SiGe HBT for low power cryogenic preamplification of a SET charge sensing circuit. The HBT-SET charge sensing circuit is shown to produce a substantial increase in SNR relative to the SET charge sensing circuit without an HBT. The gain is nonlinear when using the SET read-out configuration. Read-out behavior is simulated by using the circuit to detect random telegraph signal of a nearby charge center. The HBT-SET circuit was voltage biased to a point where the power dissipated was 0.01–5 μW; the gain was 100–2000; and the source-drain bias across SET was ~0.1–1 mV. The current gain and the noise spectrum with the HBT result in a SNR that is a factor of 10–100 larger than without the HBT at lower frequencies. The transition frequency defined by SNR = 1 has been extended by as much as a factor of 10 compared to without the HBT amplification. The increased performance is believed to be due to signal gain near the SET before a major noise source is introduced in front of the room-temperature transimpedance amplification stage.

[1]J. J. Pla, K. Y. Tan, J. P. Dehollain, W. H. Lim, J. J. L. Morton, D. N. Jamieson, A. S. Dzurak, and A. Morello, Nature **489**, 541 (2012).
[2]W. M. Witzel, M. S. Carroll, A. Morello, L. Cywiński, and S. Das Sarma, Phys. Rev. Lett. **105**, 187602 (2010).
[3]D. D. Awschalom, L. C. Bassett, A. S. Dzurak, E. L. Hu, and J. R. Petta, Science **339**, 1174 (2013).
[4]F. A. Zwanenburg, A. S. Dzurak, A. Morello, M. Y. Simmons, L. C. L. Hollenberg, G. Klimeck, S. Rogge, S. N. Coppersmith, and M. A. Eriksson, Rev. Mod. Phys. **85**, 961 (2013).
[5]J. J. L. Morton, D. R. McCamey, M. A. Eriksson, and S. A. Lyon, Nature **479**, 345 (2011).
[6]J. M. Elzerman, R. Hanson, L. H. Willems van Beveren, B. Witkamp, L. M. K. Vandersypen, and L. P. Kouwenhoven, Nature **430**, 431 (2004).
[7]R. Hanson, L. H. W. van Beveren, I. T. Vink, J. M. Elzerman, W. J. M. Naber, F. H. L. Koppens, L. P. Kouwenhoven, and L. M. K. Vandersypen, Phys. Rev. Lett. **94**, 196802 (2005).
[8]C. Barthel, D. J. Reilly, C. M. Marcus, M. P. Hanson, and A. C. Gossard, Phys. Rev. Lett. **103**, 160503 (2009).
[9]M. H. Devoret and R. J. Schoelkopf, Nature **406**, 1039 (2000).
[10]A. Morello, J. J. Pla, F. A. Zwanenburg, K. W. Chan, K. Y. Tan, H. Huebl, M. Mottonen, C. D. Nugroho, C. Yang, J. A. van Donkelaar, A. D. C. Alves, D. N. Jamieson, C. C. Escott, L. C. L. Hollenberg, R. G. Clark, and A. S. Dzurak, Nature **467**, 687 (2010).
[11]L. A. Tracy, T. M. Lu, N. C. Bishop, G. A. Ten Eyck, T. Pluym, J. R. Wendt, M. P. Lilly, and M. S. Carroll, Appl. Phys. Lett. **103**, 143115 (2013).
[12]R. J. Schoelkopf, P. Wahlgren, A. A. Kozhevnikov, P. Delsing, and D. E. Prober, Science **280**, 1238 (1998).
[13]C. Barthel, M. Kjaergaard, J. Medford, M. Stopa, C. M. Marcus, M. P. Hanson, and A. C. Gossard, Phys. Rev. B **81**, 161308 (2010).
[14]B. J. Villis, A. O. Orlov, S. Barraud, M. Vinet, M. Sanquer, P. Fay, G. Snider, and X. Jehl, Appl. Phys. Lett. **104**, 233503 (2014).

[15]M. F. Gonzalez-Zalba, S. Barraud, A. J. Ferguson, and A. C. Betz, Nat. Commun. **6**, 6084 (2015).
[16]J. Verduijn, M. Vinet, and S. Rogge, Appl. Phys. Lett. **104**, 102107 (2014).
[17]J. I. Colless, A. C. Mahoney, J. M. Hornibrook, A. C. Doherty, H. Lu, A. C. Gossard, and D. J. Reilly, Phys. Rev. Lett. **110**, 046805 (2013).
[18]A. Wallraff, D. I. Schuster, A. Blais, L. Frunzio, R.-S. Huang, J. Majer, S. Kumar, S. M. Girvin, and R. J. Schoelkopf, Nature **431**, 162 (2004).
[19]K. D. Petersson, L. W. McFaul, M. D. Schroer, M. Jung, J. M. Taylor, A. A. Houck, and J. R. Petta, Nature **490**, 380 (2012).
[20]A. R. Schmidt, E. Henry, C. C. Lo, Y.-T. Wang, H. Li, L. Greenman, O. Namaan, T. Schenkel, K. B. Whaley, J. Bokor, E. Yablonovitch, and I. Siddiqi, J. Appl. Phys. **116**, 044503 (2014).
[21]R. Vijay, M. H. Devoret, and I. Siddiqi, Rev. Sci. Instrum. **80**, 111101 (2009).
[22]B. Abdo, K. Sliwa, S. Shankar, M. Hatridge, L. Frunzio, R. Schoelkopf, and M. Devoret, Phys. Rev. Lett. **112**, 167701 (2014).
[23]J. Stehlik, Y.-Y. Liu, C. M. Quintana, C. Eichler, T. R. Hartke, and J. R. Petta, e-print arXiv:1502.01283v1.
[24]T. Gurrieri, M. Carroll, M. Lilly, and J. Levy, in *NANO'08, 8th IEEE Conference on Nanotechnology* (2008), pp. 609–612.
[25]K. Das, T. Lehmann, and A. Dzurak, IEEE Trans. Circuits Syst. I: Regul. Pap. **61**, 2816 (2014).
[26]I. T. Vink, T. Nooitgedagt, R. N. Schouten, L. M. K. Vandersypen, and W. Wegscheider, Appl. Phys. Lett. **91**, 123512 (2007).
[27]J. D. Cressler and G. Niu, *Silicon-Germanium Heterojunction Bipolar Transistors* (Artech House, 2002).
[28]J. D. Cressler and H. A. Mantooth, *Extreme Environment Electronics* (CRC Press, 2012).
[29]J. Cressler, IEEE Trans. Device Mater. Reliab. **10**, 437 (2010).
[30]L. Najafizadeh, J. Adams, S. Phillips, K. Moen, J. Cressler, S. Aslam, T. Stevenson, and R. Meloy, IEEE Electron Device Lett. **30**, 508 (2009).
[31]A. Joseph, J. Cressler, and D. Richey, IEEE Electron Device Lett. **16**, 268 (1995).
[32]F. Balestra and G. Ghibaudo, *Device and Circuit Cryogenic Operation for Low Temperature Electronics* (Kluwer Academic Publishers, 2001).
[33]E. A. Gutierrez-D, J. Deen, and C. Claeys, *Low Temperature Electronics: Physics, Devices, Circuits, and Applications* (Academic Press, 2000).
[34]At the time of publication, the manufacturer's website states that the CEL NESG3031M05 HBT is no longer in production. However, the Infineon BFP842ESD HBT had a similar biasing calibration curve at 4 K as shown in Figure 2(a).
[35]S. Mahapatra, V. Vaish, C. Wasshuber, K. Banerjee, and A. Ionescu, IEEE Trans. Electron Devices **51**, 1772 (2004).